NANO · MICRO
small

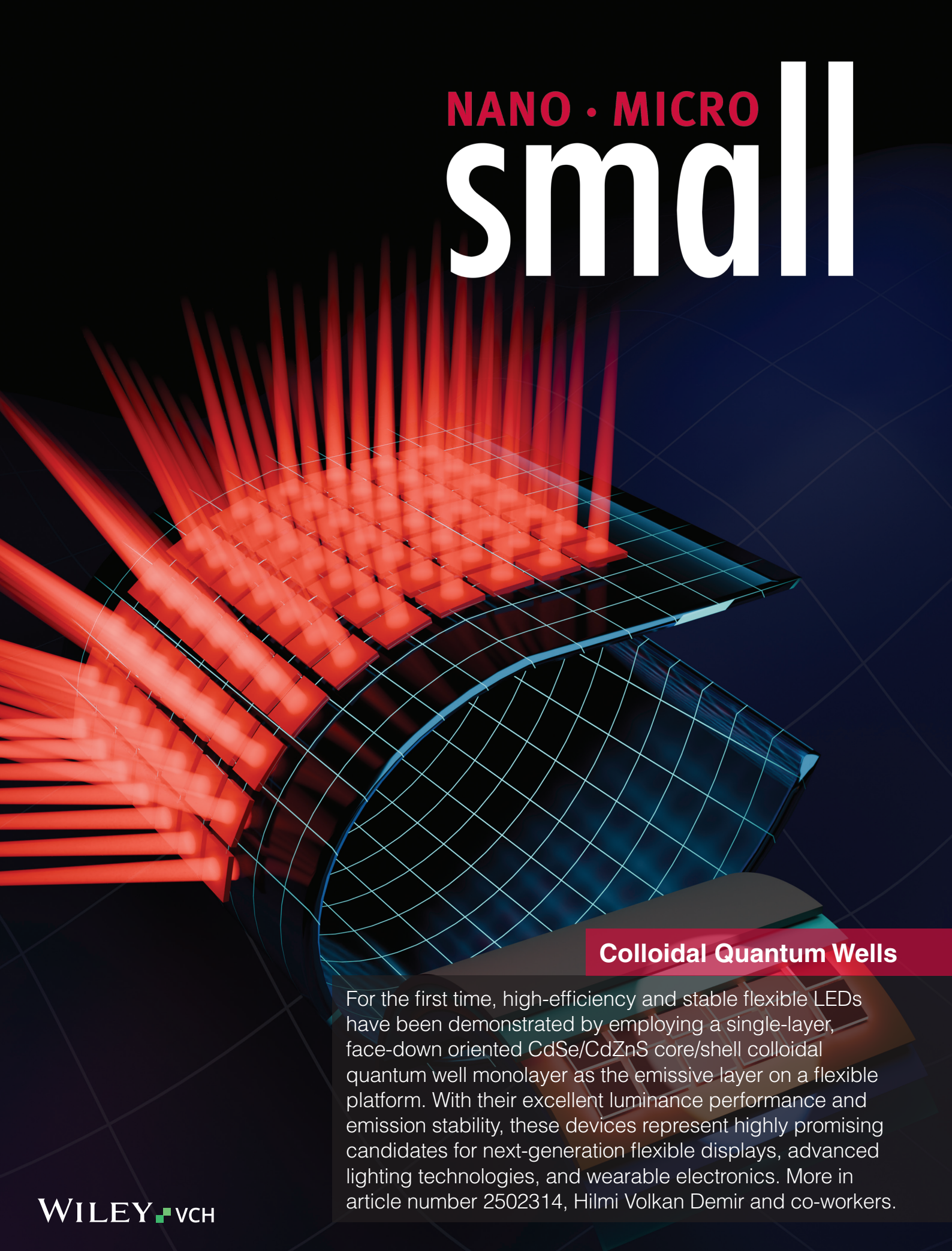

Colloidal Quantum Wells

For the first time, high-efficiency and stable flexible LEDs have been demonstrated by employing a single-layer, face-down oriented CdSe/CdZnS core/shell colloidal quantum well monolayer as the emissive layer on a flexible platform. With their excellent luminance performance and emission stability, these devices represent highly promising candidates for next-generation flexible displays, advanced lighting technologies, and wearable electronics. More in article number 2502314, Hilmi Volkan Demir and co-workers.

WILEY VCH

RESEARCH ARTICLE

NANO · MICRO small
www.small-journal.com

Flexible Colloidal Light-Emitting Diodes of Self-Assembled Quantum Well Monolayers

*Betul Canimkurbey, Furkan Isik, Savas Delikanli, Iklim Bozkaya, Emre Unal, Ahmet Tarik Isik, Zeynep Dikmen, Farzan Shabani, Ilayda Ozkan, Selin Piravadili, and Hilmi Volkan Demir**

Quasi-2D semiconductor nanocrystals, also known as colloidal quantum wells (CQWs), with their high quantum yield in the visible range, ultra-narrow emission, and in-plane oriented transition dipole moments, provide potentially an excellent platform for flexible light-emitting diodes (f-LEDs). In this study, it is proposed and demonstrated colloidal f-LEDs of a single layer face-down oriented CdSe/CdZnS core/hot injection shell-grown CQWs employed as an emissive monolayer in a flexible platform for the first time. The obtained f-LEDs are shown to be immune to a large number of bending, enabled by the use of only a single emitter layer and their configuration all being face-down in the layer. These f-LEDs exhibit a maximum external quantum efficiency of 14.12%, an intense luminance of ≈33 700 cd m^{-2}, a low turn-on voltage of <2 V, and a highly saturated red color. Here, orienting these CQWs only in face-down configuration is essential to efficient charge injection thanks to its extremely low roughness and increased outcoupling efficiency owing to in-plane oriented transition dipoles. Therefore, these f-LEDs of face-down CQW monolayers, with their excellent luminance properties and stable emission, stand out as exceptional candidates for future advanced flexible display and lighting applications as well as wearables.

1. Introduction

Semiconductor colloidal quantum wells (CQWs) have been synthesized with precise control over vertical thickness.[1–3] These CQWs, which are atomically flat and only a few monolayers thick, have been obtained with precise control in different compositions, including CdSe, CdS, and CdTe.[4] Thanks to their superior characteristics, such as ultra-narrow emission owing to their magic-sized vertical thickness, giant oscillator strength, large linear and nonlinear absorption cross-sections, anisotropic emission due to in-plane transition dipoles and near-unity photoluminescence quantum yield (PLQY),[5–8] CQWs have offered an excellent platform for light-emitting diodes (LEDs), lasers, photovoltaic devices,[9–12] Liu et al. have reported the best-performing CQW-LEDs with a high external quantum efficiency (EQE) of 19.2%.[13] A key factor for this high

B. Canimkurbey, F. Isik, S. Delikanli, I. Bozkaya, E. Unal, A. T. Isik, Z. Dikmen, F. Shabani, I. Ozkan, H. V. Demir
Department of Electrical and Electronics Engineering
Department of Physics
UNAM – Institute of Materials Science and Nanotechnology
Bilkent University
Ankara 06800, Turkey
E-mail: hvdemir@ntu.edu.sg, volkan@bilkent.edu.tr

B. Canimkurbey
Department of Physics
Polatlı Faculty of Arts and Sciences
Ankara Hacı Bayram Veli University
Ankara 06900, Turkey

The ORCID identification number(s) for the author(s) of this article can be found under https://doi.org/10.1002/smll.202502314

DOI: 10.1002/smll.202502314

S. Delikanli, E. Unal, H. V. Demir
Luminous! Center of Excellence for Semiconductor Lighting and Displays
School of Electrical and Electronic Engineering
School of Physical and Mathematical Sciences
School of Materials Science and Engineering
Nanyang Technological University
50 Nanyang Avenue, Singapore 639798, Singapore

Z. Dikmen
Faculty of Engineering
Department of Biomedical Engineering
Eskisehir Osmangazi University
Eskisehir 26040, Turkey

S. Piravadili
Material Technologies
The Scientific and Technological Research Council of Turkey (TUBITAK) – Marmara Research Center (MAM)
Gebze/Kocaeli 41470, Türkiye

performance is the exploitation of the hot-injection shell (HIS) growth of CQWs, which enables near-unity PLQY, suppression of Auger recombination, and enhanced stability, and also provides a smooth confinement potential as a result of the gradient shell. However, in the spin-coated CQW films, a significant portion of the CQWs are composed of stacks and oriented randomly relative to the substrate surface normal.[9,14] This alignment of CQWs due to stacking reduces the external quantum efficiency (EQE) in LEDs because of the low PLQY of the film due to homo-FRET (Förster resonance energy transfer) assisted exciton trapping especially when CQWs have defected subspecies, and isotropic emission.[15]

Self-assembled monolayer (SAM) films of CQWs are expected to overcome the aforementioned adverse effects that occur with the spin-coating of the CQWs. Recently, developed self-assembly technique on CQWs provides a great opportunity to implement oriented CQWs in LEDs.[16,17] The construction of highly uniform multilayered superstructures of CQWs using the self-assembly method has also been demonstrated.[18,19] This method allows for orientation-controlled deposition of CQW monolayers on various substrates with full surface coverage. Such orientation-controlled deposition of CQWs provides a uniform and densely packed film of emitters with the lowest roughness possible among the various deposition techniques[20,21] on the device layers. This extremely low roughness in the range of sub-nanometer levels is critical for obtaining efficient devices.[13,22] In addition, the self-assembly technique allows for the deposition of face-down oriented CQWs having transition dipoles sitting in-plane, which in turn enhances the light outcoupling efficiency and reduces the homo-FRET otherwise leading to nonradiative recombination. Therefore, such self-assembly techniques enabling high PLQY in film and light outcoupling efficiency are deterministic for achieving high-efficiency LEDs.[23] These face-down oriented CQWs, with their in-plane transition dipoles and extremely low film roughness, present an extraordinary platform for LEDs in different architectures on various substrates, and the LEDs having face-down oriented CQWs were demonstrated using only rigid substrates so far.[23] Flexible LEDs, especially with their ultra-thin and foldable properties,[21,22] offer a remarkable ground for implementing self-assembled CQWs. Although flexible LEDs based on solution-processed Cd-based QDs and perovskites have been investigated vigorously by several groups,[24–26] flexible LEDs based on CQWs have been explored in recent studies.[27] However, our work builds on this by demonstrating enhanced performance metrics, including superior external quantum efficiency and mechanical stability, making a significant contribution to the ongoing development of flexible optoelectronics.

In this work, we proposed and developed highly efficient and bright flexible light-emitting diodes (f-LEDs) using orientation-controlled self-assembled core/shell CQWs as a light-emitting layer for the first time. The fabricated f-LEDs are resistant to a large number of bending as a result of the use of only face-down oriented monolayer of CQWs as an emissive layer. These f-LEDs were obtained using ITO-coated flexible PET substrate and self-assembled CQWs having roughness in the range of sub-nanometer level. Owing to orientation controlled self-assembly of CQWs we could fully exploit CQWs out-of- plane directional emission, which resulted in the highest external quantum efficiency (EQE) of 14.12% among the CQW based flexible LEDs emitting in the red region[27,28] and a respectively high luminance at max EQE of 20 000 cd m^{-2}. In addition, we investigated the performance of our f-LEDs by applying strain with the help of bending the devices consecutively, and the performance remained almost the same after five hundred cycles. These results indicate the extraordinary potential of oriented CQW-based f-LEDs for future optoelectronic applications.

2. Results and Discussion

Colloidal CdSe/CdZnS core/HIS CQWs were synthesized following the reported procedures with slight modifications for use in our flexible LEDs.[17,29] Briefly, the CdZnS shell layer was grown on the seed 4.5-monolayer thick CdSe CQWs by introducing the cadmium and zinc precursors at room temperature and constantly adding the sulfur precursor at higher temperatures. It is worth noting that high temperatures are needed for the shell growth due to the high decomposition temperature of our sulfur precursor, octanethiol. Further details of the synthesis are given in the Supporting Information. The gradient shell in these CQWs helps isolate the photogenerated carriers from nonradiative surface trap sites by confining the carriers in the core and suppressing the lattice mismatch between the core and the shell layers to prevent the formation of nonradiative interface defect sites. In addition, such a wide bandgap gradient shell grown on core nanocrystals efficiently reduces the fast nonradiative Auger recombination.[30] We synthesized CdSe/CdZnS core/HIS CQWs in square shape since it was shown previously that square-shaped core/HIS CQWs perform better in LEDs than rectangular core/HIS CQWs.[23,29] These square-shaped core/HIS CQWs have a side length of ≈10.5 nm, as seen from the transmission electron microscopy (TEM) image in **Figure 1a**. The PL peak wavelength of these CdSe/CdZnS core/HIS CQWs is located at 648 nm with a full-width-at-half-maximum (FWHM) of 27 nm, as presented in Figure 1b, and their PLQY is ≈89%, which is measured by an integrating sphere upon 400 nm excitation. Unfortunately, these CdSe/CdZnS core/HIS CQWs as-synthesized were passivated with oleic acid (OA) and oleylamine (OLA) ligands having a long hydrocarbon tail, which is destructive for the charge transport by extending the hopping distance of carriers in a device.

Thus, we replaced the native OA and OLA ligands having long tails with a shorter 2-ethylhexane-1-thiol (EHT) ligand to facilitate efficient charge transport. The role of surface ligands is critical, as they not only ensure favorable solubility for solution-processed fabrication but also improve the possibility of charge recombination and energy transfer between the charge transport layers and CQW layers. Our recent study demonstrates that utilizing short-chain 2-ethylhexane-1-thiol (EHT) as a capping ligand offers several advantages, including reducing the hole injection potential barrier.[23]

We performed NMR and FTIR spectroscopies to probe the efficiency of the ligand exchange on our CdSe/CdZnS CQWs. ^{1}H NMR spectra of EHT ligand, OLA, and CdSe/CdZnS CQWs after ligand exchange (LE) procedure with EHT are given in Figure 1e. After ligand exchange, a weak OLA alkene peak appears at 5.26 ppm, and CH_2-N protons of OLA can be observed at 2.71 ppm as a weak peak while CH_2-S protons of EHT can be

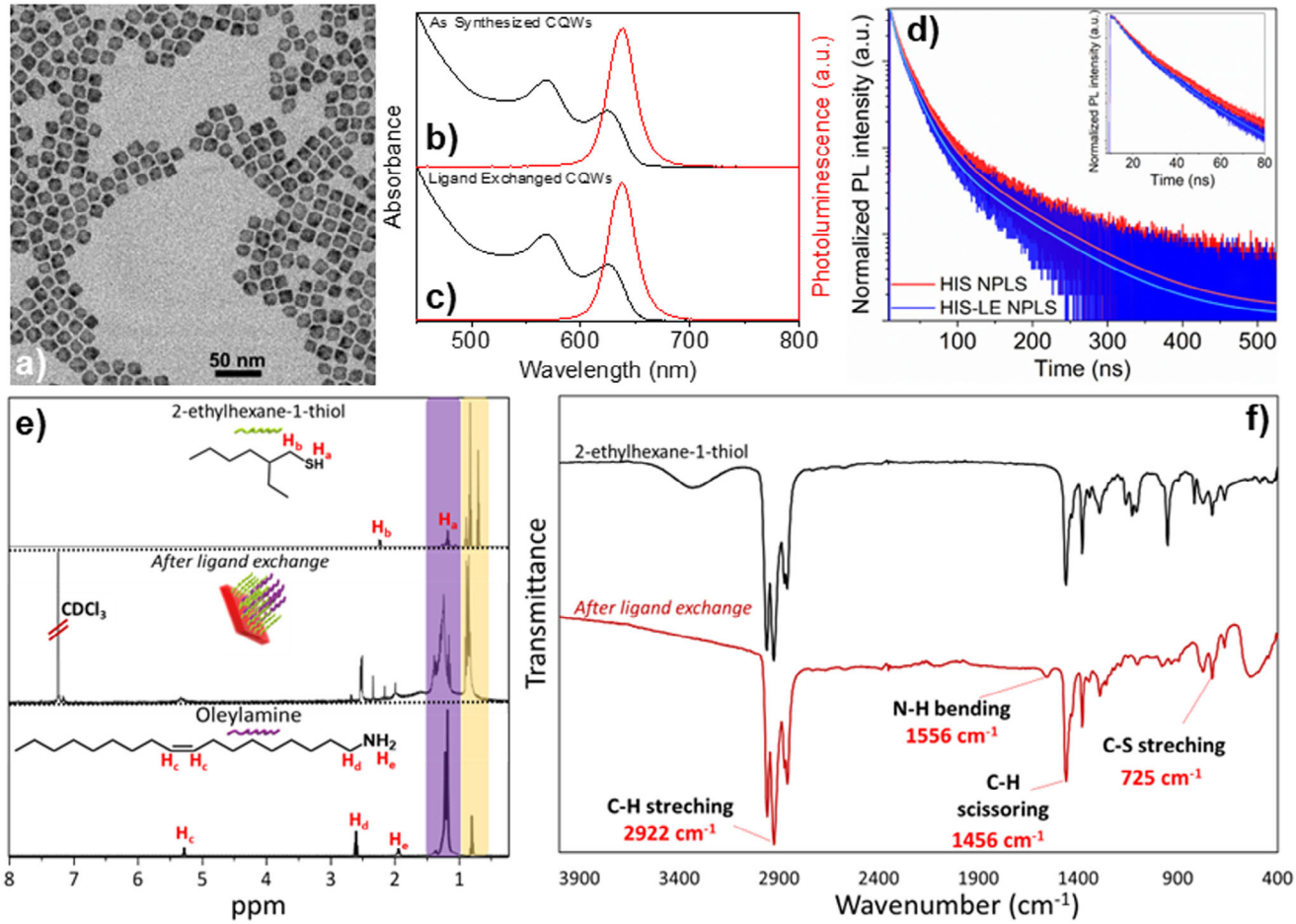

Figure 1. a) TEM image of the CQWs with 4 ML of CdSe/ZnS HIS having a square shape. b) Absorbance and PL spectra curves of these HIS grown CQWs. c) Absorbance and PL spectra curves of HIS CQWs after the ligand exchange. d) Time-resolved fluorescence (TRF) decay curves and their corresponding fitted curves for the CdSe/CdZnS core/HIS CQWs in solution before and after the ligand exchange (LE) at their PL peak wavelengths. The inset shows the zoom-in of the same graph at shorter times. e) ^{1}H NMR spectra of EHT, OLA, and CdSe/CdZnS CQWs after the ligand exchange. f) ATR-IR spectra of EHT (black line) and CdSe/CdZnS CQW after the ligand exchange with EHT (red line).

observed clearly at 2.53 ppm. Our ^{1}H NMR spectrum of ligand-exchanged CdSe/CdZnS CQWs clearly shows that these CQWs are capped with mostly EHT ligands and partially with OLA after ligand exchange. The ligand exchange was also probed by functional group analysis to verify the successful attachment of EHT to the core/shell CQWs with attenuated total reflection infrared (ATR-IR) spectroscopy. Fourier transform infrared (FTIR) spectra of EHT ligands and CdSe/CdZnS CQW after ligand exchange are given in Figure 1f. —OH peak observed at 3321 cm^{-1} is attributed to hydroxyl asymmetrical stretching vibration of water adsorbed by the —SH group of EHT. Due to the fact that the —SH group of EHT is converted into —S—Cd or —S—Zn groups after ligand exchange, its hygroscopic property decreases dramatically, and therefore, the —OH peak is not observed. Signals of asymmetric and symmetric vibrations of CH_2 groups of OLA and EHT are observed at 2922 and 2,858 cm^{-1} as sharp peaks because of the hydrocarbon chain of oleylamine and EHT. The peak at 1,556 cm^{-1} observed after ligand exchange belongs to the N—H bending of the OLA ligand.[31,32] The C—S stretching peak of the EHT ligand is at 725 cm^{-1}. EHT replaces oleic acid and maintains good dispersion of the CQWs. These results from FTIR measurements, together with the results from NMR measurements, indicate that our CdSe/CdZnS CQWs are largely passivated by the EHT ligands with minor contributions from OLA ligands. It can be seen from Figure 1c that the PL emission peak and excitonic transition peak positions of the CQWs remained almost the same after the ligand exchange. In addition, we performed time-resolved fluorescence (TRF) spectroscopy to probe if the ligand exchange affects the recombination kinetics in CdSe/CdZnS CQWs. The photoluminescence decay curves of CdSe/CdZnS CQWs before and after the ligand exchange (LE) are given in Figure 1d. We employed a tri-exponential decay function for the fitting of the TRF decay curves. The lifetime components, the amplitude of each component, and intensity-averaged lifetimes are given in Table S1 (Supporting Information). The CQWs passivated with the original long chain oleic acid and oleylamine ligands exhibit a slightly longer intensity-averaged lifetime (τ_{avg}) of 30.2 ns compared to that of LE-CQWs (26.9 ns), which confirms no drastic change in the recombination behavior of the CQWs. The lifetime components provided in Table S1 (Supporting

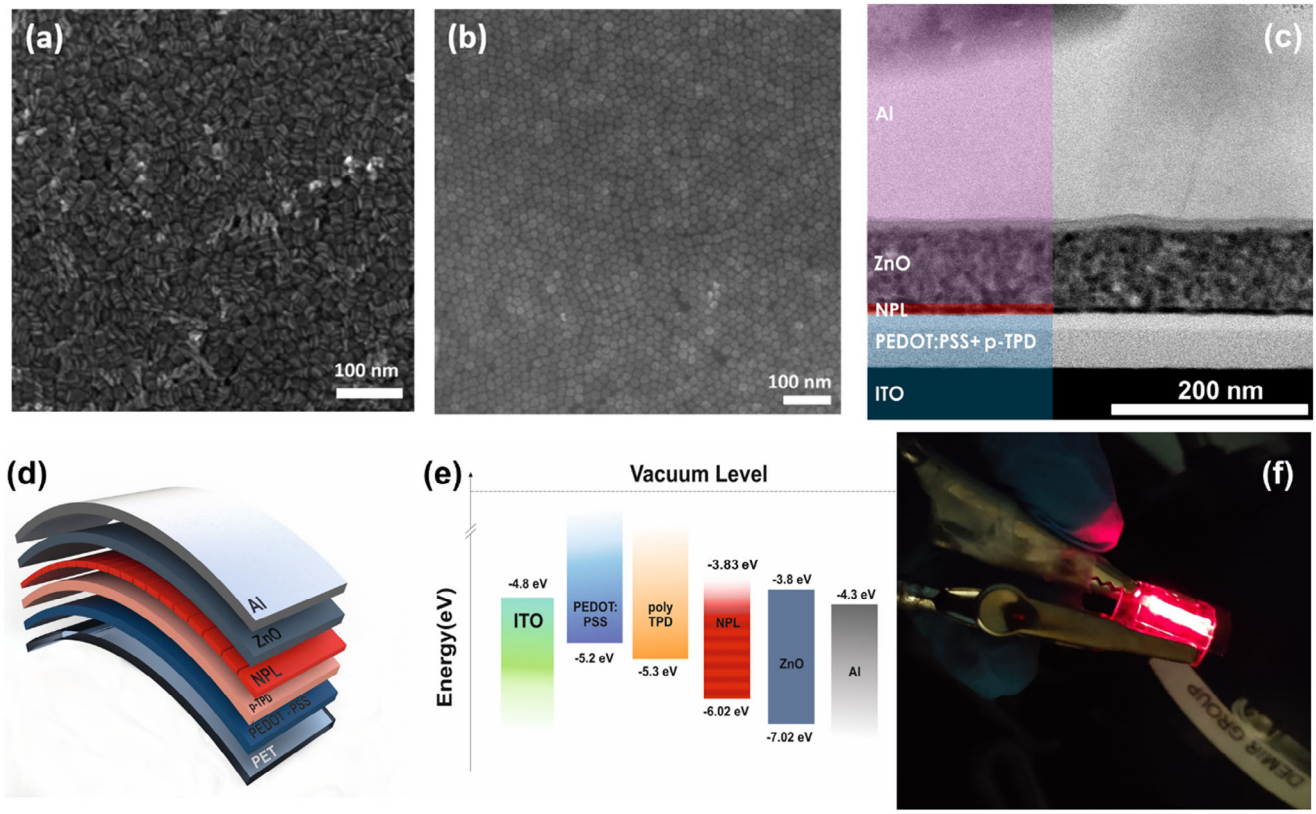

Figure 2. a) Scanning electron microscopy (SEM) image of the spin-casted film of CQWs. b) SEM image of the all-face-down self-assembled monolayer of CQWs on the device's layers. c) Transmission electron microscopy (TEM) cross-sectional image of the device containing the face-down oriented hot-injection shell (HIS) grown CQW SAM, marked with its energy-dispersive X-ray spectroscopy (EDAX) mapping. d) Schematic illustration of the device. e) Energy diagram of each layer deposited in the flexible LED device fabrication.[27] f) Image of a working fabricated flexible CQW-LED device under 5 V.

Information) indicate that the share of the fastest channel for LE-CQWs, which is known to contribute the most of the nonradiative recombination,[33] is only increased by 3%, and the change in the share of the two other channels was below 2%. As the new ligands have a shorter length than the original ones, the decreased lifetime is probably due to the change in the dielectric felt by the carriers.[34] The observation further confirms the potency of our ligand exchange method, where the integrity of the CQWs is maintained at the highest level. As a result, the recombination behavior of the CQWs did not change, and the PLQY of the CQWs was kept near unity.

To investigate their film formation, we prepared films of these ligand-exchanged CdSe/CdZnS CQWs on silicon substrates using spin-coating and self-assembly techniques (details in Supporting Information). **Figure 2**a,b show the scanning electron microscopy (SEM) images of the obtained films of ligand exchanged CdSe/CdZnS CQWs on silicon substrates by spin-coating and self-assembly techniques, respectively. Briefly, spin-coated films of CQWs were obtained by using 25 mg mL^{-1} of CQWs in hexane with an rpm of 2500, while the self-assembly of all face-down oriented CQWs was performed by employing acetonitrile, which has a high polarity index and a matching polarity to the EHT ligand, as a subphase. The CQW assembly configuration depends on the interaction potential between the CQWs and the liquid interface.[35] We dropped 25 µL of a hexane solution containing CQWs with a concentration of ≈8 mg mL^{-1} onto the acetonitrile, resulting in a nearly complete coverage of the liquid-air interface by a monolayer of CQWs after the evaporation of the hexane. The appearance of a clear mosaic-like structure only in the self-assembled film proves the successful deposition of a single layer of face-down oriented CQWs. In addition, we performed atomic force microscopy (AFM) measurements on these films to investigate the surface roughness of the films, which is a critically important parameter for device applications. The roughness of the SAM films is 0.8 nm (as presented in Figure S7a, Supporting Information), which suggests that SAM films are highly advantageous compared to the spin-coated films having roughness of ≈3 nm (as given in Figure S7b, Supporting Information). Typically, the self-assembled films of CQWs form a monolayer with a thickness equivalent to the height of the CQWs.

Upon optimization of the CdSe/ZnS HIS CQW films through self-assembly, the full potential of CQW-f-LEDs was exploited on the flexible indium tin oxide (ITO)-coated polyethylene terephthalate (PET) substrates. Figure 2d illustrates the schematic of the flexible CQW-f-LED device on a PET substrate. The detailed fabrication process of the CQW-f-LED device is described in the Supporting Information. Our CQW-f-LED device consists of ITO as an anode, poly(ethylene dioxythiophene):polystyrene sulphonate (PEDOT:PSS) as the hole injection layer, poly (N,N9-bis(4-butyl phenyl)-N,N9-bis(phenyl)-benzidine) (p-TPD) as the hole

transport layer, self-assembled CQWs as an emitting layer, zinc oxide (ZnO) as the electron transport layer, and aluminum (Al) as a cathode as shown in Figure 2d. Layers were deposited using spin-coating on ITO except for the Al cathode, which was deposited by thermal evaporation.

Considering the influence of the coating technique and coated film on the morphology of ligand-exchanged spin-coated (LES) and ligand-exchanged self-assembled (LESA) films, it is reasonable to anticipate that these factors will also affect the charge transport and recombination processes in f-LEDs. We obtained 2 different f-LEDs employing ligand-exchanged CQWs in the emitting layer using spin-coating and self-assembly techniques. These 2 f-LEDs were labeled according to their CQW layer. Spin-coated LE-CQW-f-LED has a CQW layer obtained using ligand-exchanged CQWs by applying the spin-coating method, and oriented LE-CQWf-LED has a CQW layer obtained using ligand-exchanged CQWs by applying the self-assembly technique. We took a cross-sectional TEM image of the most promising CQW-based f-LED between these two, which is the oriented LE-CQW-f-LED due to its CQW layer having face-down orientation with in-plane transition dipoles enhancing the outcoupling efficiency.

All the deposited layers are clearly seen on the cross-sectional TEM image presented in Figure 2c. This cross-sectional TEM image is profiled with its energy-dispersive X-ray spectroscopy (EDAX), which identifies elemental compositions of all deposited layers in the device. The thickness of the electron transport ZnO layer is ≈40 nm, while the thickness of the hole injection PEDOT:PSS and hole transport p-TPD layers are ≈50 nm. The thickness of the CQW film obtained from the TEM cross-section is ≈4.0±0.5 nm. This thickness is very similar to the thickness of core–shell CQWs,[23] which is another indication of that this CQW film contains only a monolayer of face-down oriented CQWs.

The energy level diagram presented in Figure 2e illustrates that the HOMO-LUMO energies of the materials in the LED structure were aligned for charge injection between the anode and cathode sides of the device, thanks to the low energy barriers between the layers. Moreover, the use of a high-workfunction PEDOT:PSS layer can further reduce the injection barriers between ZnO and CQW emitter, resulting in lower ohmic loss and operating voltage. The efficient electron injection responsible for the decreased turn-on voltage of the LED device is facilitated by the well-matched high-lying lowest unoccupied molecular orbital levels of Al and ZnO with the LUMO level of CdSe/CdZnS CQWs.

Additionally, the HOMO energy level of CdSe/CdZnS CQWs is compatible with the HOMO energy level of p-TPD, allowing efficient hole transport from ITO to the emissive layer. This effective transportation of electrons and holes leads to improved luminance via efficient recombination of the charge carriers in the emissive layer of the conventional LEDs. When a forward bias is applied to the device that has been fabricated, red electroluminescence (EL) can be observed. The voltage-dependent normalized EL spectra of CQWs are illustrated in **Figure 3a**.

Figure 3a clearly shows discernible emission that originates from the CdSe/CdZnS monolayer. The increase in voltage is accompanied by an increase in the EL intensity. Moreover, there is almost no shift in the peak wavelength of the EL spectrum when the voltage was changed from 0 to 10 V. The emission of the oriented LE-CQW-LED under external applied voltage exhibits a peak at 653.8 nm with an FWHM of 27 nm as presented in Figure 3a. Compared with the PL spectrum, it is obvious that the PL and EL spectra coincide nicely, indicating that the energy transfer from smaller to larger CQWs in the emission layer is suppressed effectively.[36] In addition, the LEDs exhibit a single EL emission peak without other peaks from any charge transport materials. This further confirms that CQWs are the primary exciton recombination centers, and there is a balanced charge carrier transport during the device operation.[37] Figure 3a depicts an inset photograph of a flexible LED under operating conditions. The f-LED device contains two active areas, each with aluminum cathodes measuring 18.75 mm^2. The device is shown in a bent state and operated at an applied voltage of 5 V, demonstrating its flexibility and potential for use in various applications. Even in the bent state, a homogeneous and contiguous light emission in the red spectral region over the whole active area was observed. Our device displays pure color well-located in the red region with (x, y) tristimulus coordinates of (0.7053, 0.2942), a color point which is relatively close to the spectral locus of (0.7053, 0.2942) known as saturated red color, as presented in Figure 3b. This CIE coordinate for red is ideal for new generation ultra-high-definition television (UHDTV) applications to increase the color gamut.[21,38]

The current density–voltage–luminance (J–V–L) characteristics of our flexible LEDs are analyzed in Figure 3c. This figure shows the impact of the coating technique and the resulting CQW morphology on the LED performance. At the same applied voltage, the measured current is lower for the spin-coated LE-CQW-LED than the self-assembled LE-CQW-LED. This can be attributed to the thinner and more homogeneous film nature of self-assembled LE-CQW-LED facilitating more efficient charge injection and transport. They are exhibiting the typical diode- characteristics, where the current increases exponentially above ≈1.8 V (turn-on voltage of the electroluminescence (EL)). The current densities in the range of several ≈65–335 mA cm^{-2} at 8.0 V is in good agreement with the literature for QD-LEDs[39] and perovskite LEDs.[40] Our oriented LE CQW-LEDs have been found to show higher current densities and higher brightness compared to the spin-coated LE-CQW-LEDs. The luminance of the oriented LE-CQW-LED reaches 33 700 cd m^{-2} while that of the spin-coated LE-CQW-LED is 23 308 cd m^{-2}. This level of luminance is higher than the previous record value of 13 644 cd m^{-2} for perovskite light-emitting devices at a similar wavelength.[41] It is reported that flexible LEDs on ITO-coated polyethylene naphthalate (PEN) substrate with WS_2 monolayer material as an active layer lead to red light emission with the same spectral position and active area of 6 mm^2.[42] With a turn-on voltage <3 V, this WS_2 device reaches a luminance of ≈1 cd m^{-2} at 9 V.[42] Here the studied flexible LEDs on ITO-coated PET substrate with a CQW layer as an emissive layer, having an EL peak position of 648 nm and an active area of 18.75 mm^2, feature a smaller turn-on voltage of <2 V and a significantly higher luminance level of 23 308 cd m^{-2}, 5 orders of magnitude stronger. The turn-on voltage in our devices is as low as ≈2 V which is lower than all of the previous reports at the same wavelength.[42,43] The maximum EQE of the oriented LE-CQW-LED, which is 14.12%, is considerably larger than that of the spin-coated LE-CQ-LED, which is 8.51%. The lower EQE of spin-coated LE-CQ-LED can be attributed to increased surface roughness and film inhomogeneity, which leads

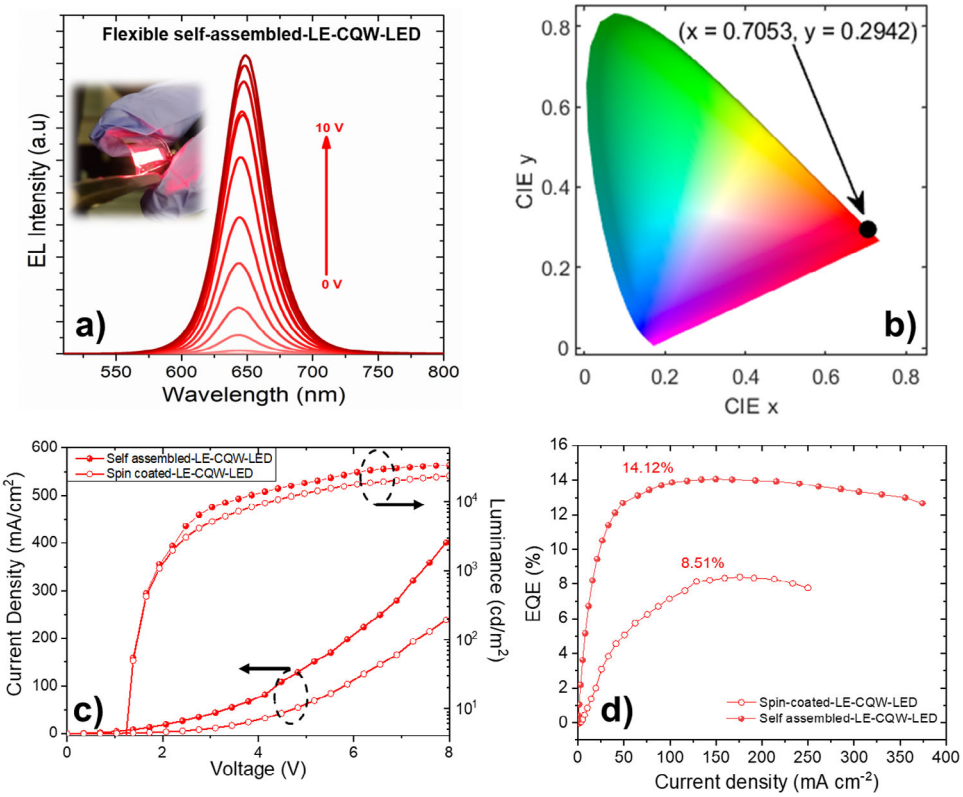

Figure 3. a) Voltage-dependent normalized electroluminescence (EL) spectra of the self-assembled LE-CQW-LEDs taken from an unstrained device. b) CIE gamut of the self-assembled LE-CQW-LEDs. c) Current density–voltage graph of the spin-coated LE-CQW-LED and self-assembled LE-CQW-LEDs. d) EQE-voltage graph of the spin-coated LE-CQW-LED and self-assembled LE-CQW-LEDs.

to charge trapping and charge imbalance. The oriented LE-CQW LED reaches its maximum EQE at 5 V and exhibits a slight roll-off after that and reaches 12.30% at 8 V as the luminance increases from 18 000 to 33 700 cd m^{-2}. This slight roll-off suggests that the device has a balanced and efficient charge injection.[41] This peak EQE of 14.12% represents the highest reported value for CQW-QLEDs.[27] The high EQE is maintained across a wide range of current densities, with EQE > 13% observed between 64 and 355 mAcm^{-2}, corresponding to a brightness range of 11 000–33 000 cd m^{-2}. Even at a current density of 374 mAcm^{-2}, an EQE greater than 12% is sustained. The low-efficiency roll-off of this device, which significantly exceeds previous results for high-efficiency flexible CQW-LEDs (peak EQE of 14.12%), is higher than the previous best results,[27] highlighting the potential of our QLEDs for high-power applications. The much higher luminance and EQE observed in the oriented LE-CQW-LED compared to the spin-coated LE-CQW-LED can be attributed to the higher outcoupling efficiency as a result of the face-down oriented CQWs having strong in-plane transition dipoles leading directional emission compared to that of the spin-coated LE-CQWs having randomly oriented CQWs. It was shown in CQW-LEDs fabricated on rigid glass substrates that the outcoupling efficiency of the LED device with orientation-controlled film is 34%, while that of the LED device with the spin-coated film is 22%.[23] This improvement in the outcoupling efficiency may lead to a 54% improvement in the EQE, which is close to our 56% improvement in the EQE with the usage of the oriented LE-CQWs in the LED (compared to the spin-coated LED). Lifetime measurements at a constant driving current density of ≈30 mAcm^{-2}, corresponding to an initial luminance (L_n) of 5 000 cd m^{-2} (at an EQE above 10%), showed a half-lifetime (T_{5n}, the time required for luminance to decrease to $L_n/2$) of 14 h (Figure S11, Supporting Information). By applying the equation $L_n{}^nT_{5n} = L_1{}^nT$,[44–46] with an acceleration factor of n = 1.5,[44] we calculated T_{5n} at an initial luminance of 100 cd m^{-2}[47] as ≈5,300 h. Our flexible CQW-LEDs outperforms most of the flexible QD-LEDs and perovskite-LEDs in terms of device lifetime and efficiency[27,48–61] highlighting the significant advancements in both performance and device longevity achieved in this work. The high EQE is maintained across a wide range of current densities, with EQE > 13% observed between 64 and 355 mAcm^{-2}, corresponding to a brightness range of 11 000–33 000 cd m^{-2}.

To investigate the flexed performance of our flexible LEDs under mechanical bending stress, we induced compressive in-plane strain on the oriented LE-CQW-LED under operating conditions, as shown in **Figure** 4a. To perform the mechanical bending of our oriented LE-CQW LEDs on a flexible PET substrate, the LEDs were clamped and bent between two clamps. There were two active devices on each substrate, each having an area of 18.75 mm^2. As shown in Figure 4a, x is an adjustable distance and l is the length of the side of the device used for the mechanical bending.

Figure 4b shows the electroluminescence from the oriented LE-CQW-LED at an applied voltage of 5 V up to 500 bending

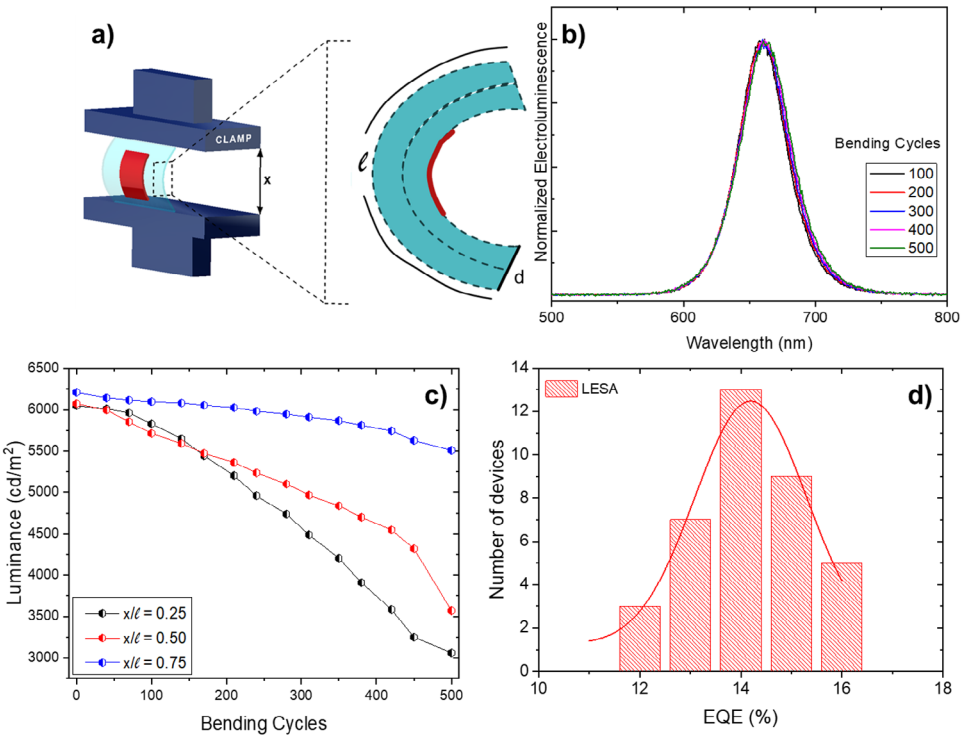

Figure 4. a) Schematic illustration of the measurement setup of the induced compressive in-plane strain in the oriented LE-CQW-LED. b) Normalized EL spectra under different bending cycles at an applied voltage of 5 V with different x/l. c) Luminance as a function of the bending cycles at an applied voltage of 5 V. d) Histograms of peak EQEs for the devices with LESA.

cycles with an x/l of 0.25. The experimental results indicate that the electro-optic and wavelength characteristics remained almost the same even after 500 bending cycles with an x/l of 0.75. This flexibility is possible because the f-LEDs are designed to be very thin, with a total thickness of 4 µm, using only a single monolayer of CQWs, all in face-down orientation. Over the active area, very uniform light emission in the red spectral region was observed even in the bent state as shown in Figures 2f, and 3a. As also presented in Figure 4c, the luminance of the oriented LE-CQW-LED decreases only 12% after 500 cycles for the case of x/l of 0.75, showing the great potential of flexible LEDs based on CQWs. Furthermore, the solution-processing protocol used in fabricating these devices has demonstrated excellent reproducibility. As illustrated by the histograms for 44 devices from five batches (Figure 4d), the high average peak EQE of 12.3% and the low relative standard deviation of 3.5% are particularly promising.[13,22]

As depicted in **Figure 5**, back-focal plane (BFP) images of the face-down self-assembled films and spin-coated were fitted with the model reported in the work of Shendre et al.[62] Our results show an IP dipole ratio of 91% in our face-down oriented film, indicating a highly directional OP emission. These findings are consistent with literature reports, such as those by Scott et al.[63] and Shendre et al.[62] who documented IP emission ratios of 95% (4.5 ML CdSe CQWs) and 91%(CdSe/CdS@CdZnS core/crown@alloyed shell CQWs), respectively, for face-down self-assembled CQWs. On the other hand, the IP dipole ratio for spin-coated films, as shown in Figure 5b, is 67%, indicating almost isotropic emission.

The marked difference in IP and OP dipole ratios between the face-down self-assembled and spin-coated films underscore the enhanced alignment and uniformity, which is achieved through the self-assembly process. The superior TDM distribution observed in the face-down self-assembled films correlates with their higher external quantum efficiency (EQE) due to enhanced out-coupling efficiency. Therefore, the TDM distribution data presented in Figure 5 validate the advantages of our face-down self-assembly technique over spin-coating.

The orientation-controlled self-assembly of colloidal quantum wells (CQWs) is pivotal in the exploitation of out-of-plane directional emission of CQWs, thereby improving light extraction and the efficiency of light-emitting devices. The integration of optimized device structures and advanced self-assembly processes have led to significant improvements in the performance of CQW-based light-emitting devices.[28,64,65] For instance, Dehghanpour Baruj et al. reported that solution-processed LEDs incorporating a monolayer of face-down oriented CQWs achieved an EQE of 18.1%, which was attributed to enhanced photon out-coupling efficiency resulting from the high degree of in-plane transition dipole moments.[64] More recently, Zhu et al., following the same self-assembly approach, achieved record high EQE of 26.9%, which showcases the utilization of directional emission of CQWs to overcome the out-coupling limitation.[28] These developments underscore the critical role of orientation-controlled self-assembly for advanced CQW-based optoelectronic applications.[19] Furthermore, employing a single layer face-down oriented CQWs reduces inter-CQW charge hopping, thereby improves charge injection efficiency. Increased emitter layer

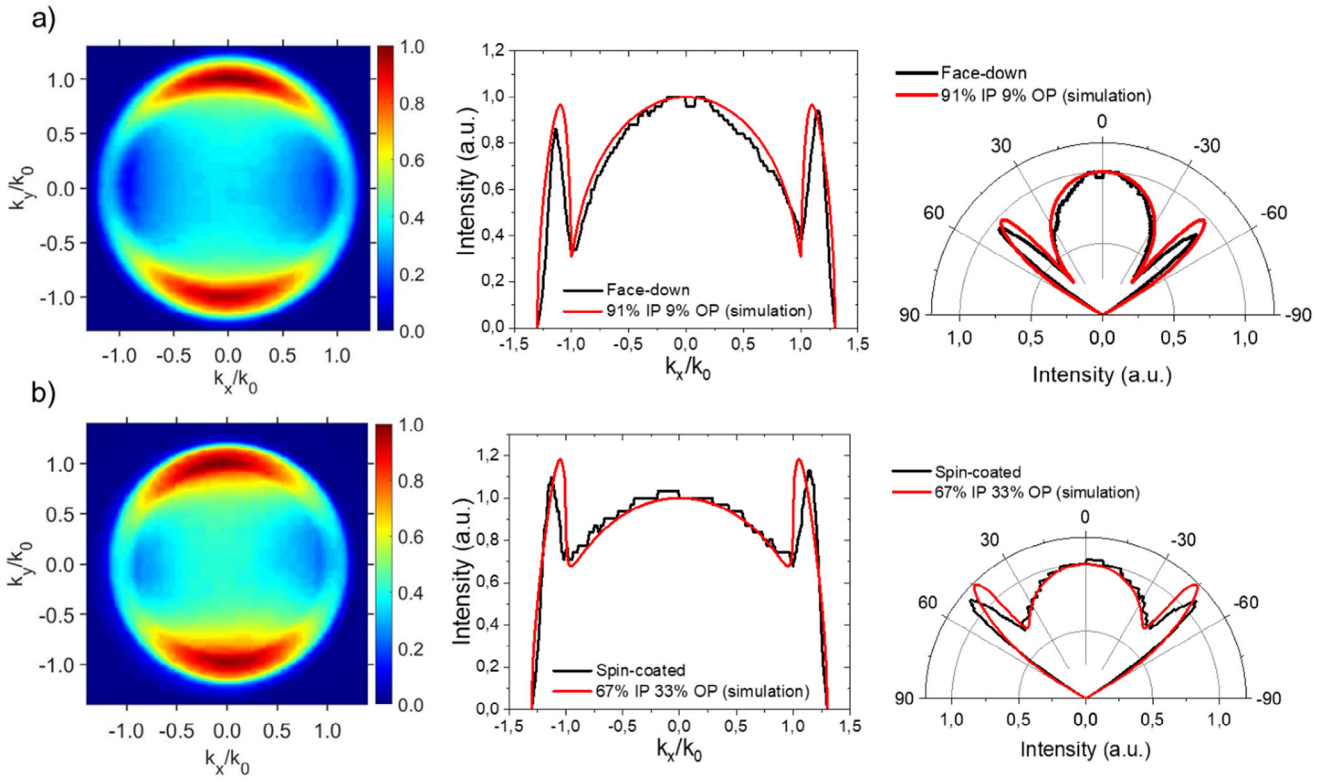

Figure 5. Emission profile, k-space, and angle (θ) dependent p-polarized emission intensity profile of p-polarized spectra, respectively a) self-assembled monolayer film on a quartz substrate with 91% IP TDMs fitting curve and b) spin-coated film on a quartz substrate with 67% IP TDMs curve.

thickness results in charge injection limitations, impairing uniform charge carrier distribution across the layer, which would result in charge imbalance and non-uniformity, and hence non-radiative Auger recombination.

3. Conclusion

A new class of flexible LEDs of self-assembled colloidal quantum wells has been developed to exploit its efficient charge injection owing to its extremely low roughness and high outcoupling efficiency as a result of the in-plane oriented transition dipoles. These flexible CQW-LEDs fabricated on plastic substrates exhibit an external quantum efficiency of 14.12% and an intense luminance of ≈33 700 cd m^{-2}. In addition, the performance of the fabricated f-LEDs varies only slightly (12% after 500 cycles for the case of x/l of 0.75) under mechanical bending stress after hundreds of cycles of bending. Therefore, these f-LEDs emerge as exceptional candidates for future advanced flexible display and lighting applications, for example in weareables, with their excellent luminance properties and stable emission. These findings indicate the great potential of the self-assembled CQW monolayers in ultrathin, scalable, and flexible optoelectronics.

Supporting Information

Supporting Information is available from the Wiley Online Library or from the author.

Acknowledgements

The authors gratefully acknowledge the financial support in part from the Singapore Agency for Science, Technology and Research (A*STAR) MTC program under grant number M21J9b0085, Ministry of Education, Singapore, under its Academic Research Fund Tier 1 (MOE-RG62/20), and in part from TUBITAK 119N343, 121C266, 121N395 and 20AG001. H.V.D. also acknowledges support from TUBA- Turkish Academy of Sciences and TUBITAK 2247-A National Leader Researchers Program (121C266). B.C. acknowledges support from TUBITAK 2218 National Postdoctoral Research Fellowship Program (120C219) and TUBITAK 124F030.

Conflict of Interest

The authors declare no conflict of interest.

Data Availability Statement

The data that support the findings of this study are available from the corresponding author upon reasonable request.

Keywords

colloidal nanoplatelets, colloidal quantum wells, flexible light-emitting devices, orientation control, self-assembly

Received: February 21, 2025
Revised: April 7, 2025
Published online: May 3, 2025

[1] Y. Altintas, K. Gungor, Y. Gao, M. Sak, U. Quliyeva, G. Bappi, E. Mutlugun, E. H. Sargent, H. V. Demir, *ACS Nano* **2019**, *13*, 10662.
[2] D. V. Talapin, J. S. Lee, M. V. Kovalenko, E. V. Shevchenko, *Chem. Rev.* **2010**, *110*, 389.
[3] J. Joo, J. S. Son, S. G. Kwon, J. H. Yu, T. Hyeon, *J. Am. Chem. Soc.* **2006**, *128*, 5632.
[4] S. Ithurria, M. D. Tessier, B. Mahler, R. P. Lobo, B. Dubertret, A. L. Efros, *Nat. Mater.* **2011**, *10*, 936.
[5] U. Resch-Genger, M. Grabolle, S. Cavaliere-Jaricot, R. Nitschke, T. Nann, *Nat. Methods* **2008**, *5*, 763.
[6] M. Olutas, B. Guzelturk, Y. Kelestemur, A. Yeltik, S. Delikanli, H. V. Demir, *ACS Nano* **2015**, *9*, 5041.
[7] M. D. Tessier, C. Javaux, I. Maksimovic, V. Loriette, B. Dubertret, *ACS Nano* **2012**, *6*, 6751.
[8] A. Yeltik, S. Delikanli, M. Olutas, Y. Kelestemur, B. Guzelturk, H. V. Demir, *J. Phys. Chem. C.* **2015**, *119*, 26768.
[9] S. Delikanli, G. N. Yu, A. Yeltik, S. Bose, T. Erdem, J. H. Yu, O. Erdem, M. Sharma, V. K. Sharma, U. Quliyeva, S. Shendre, C. Dang, D. H. Zhang, Z. C. Sum, W. J. Fan, H. V. Demir, *Adv. Funct. Mat.* **2019**, *29*, 1901028.
[10] C. She, I. Fedin, D. S. Dolzhnikov, P. D. Dahlberg, G. S. Engel, R. D. Schaller, D. V. Talapin, *ACS Nano* **2015**, *9*, 9475.
[11] F. Fan, P. Kanjanaboos, M. Saravanapavanantham, E. Beauregard, G. Ingram, E. Yassitepe, M. M. Adachi, O. Voznyy, A. K. Johnston, G. Walters, *Nano Lett.* **2015**, *15*, 4611.
[12] I. J. Kramer, E. H. Sargent, *ACS Nano* **2011**, *5*, 8506.
[13] B. Liu, Y. Altintas, L. Wang, S. Shendre, M. Sharma, H. Sun, E. Mutlugun, H. V. Demir, *Adv. Mater.* **2020**, *32*, 1905824.
[14] W. D. Kim, D. Kim, D. E. Yoon, H. Lee, J. Lim, W. K. Bae, D. C. Lee, *Chem. Mater.* **2019**, *31*, 3066.
[15] O. Erdem, M. Olutas, B. Guzelturk, Y. Kelestemur, H. V. Demir, *J. Phys. Chem. Lett.* **2016**, *7*, 548.
[16] B. T. Diroll, *J. Mat. Chem. C.* **2020**, *8*, 10628.
[17] Z. Dikmen, A. T. Isik, I. Bozkaya, H. Dehghanpour Baruj, B. Canimkurbey, F. Shabani, M. Ahmad, H. V. Demir, *Nanoscale* **2023**, *15*, 9745.
[18] O. Erdem, S. Foroutan, N. Gheshlaghi, B. Guzelturk, Y. Altintas, H. V. Demir, *Nano Lett.* **2020**, *20*, 6459.
[19] O. Erdem, K. Gungor, B. Guzelturk, I. Tanriover, M. Sak, M. Olutas, D. Dede, Y. Kelestemur, H. V. Demir, *Nano Lett.* **2019**, *19*, 4297.
[20] B. Q. Liu, S. Delikanli, Y. Gao, D. Dede, K. Gungor, H. V. Demir, *Nano Energy* **2018**, *47*, 115.
[21] J. Song, O. Wang, H. Shen, Q. Lin, Z. Li, L. Wang, X. Zhang, L. S. J. Li, *Adv. Funct. Mat.* **2019**, *29*, 1808377.
[22] Y. Shirasaki, G. J. Supran, M. G. Bawendi, V. Bulovic, *Nat. Photonics* **2013**, *7*, 13.
[23] H. D. Baruj, I. Bozkaya, B. Canimkurbey, A. T. Isik, F. Shabani, S. Delikanli, S. Shendre, O. Erdem, F. Isik, H. V. Demir, *Small* **2023**, *19*, 2206582.
[24] K. Yang, F. Li, Y. Liu, Z. Xu, Q. Li, K. Sun, L. Qiu, Q. Zeng, Z. Chen, W. Chen, W. Lin, H. Hu, T. Guo, *ACS Appl. Mater. Interfaces* **2018**, *10*, 27374.
[25] Y. Yao, H. Yu, Y. Wu, Y. Lu, Z. Liu, X. Xu, B. Ma, Q. Zhang, S. Chen, W. Huang, *ACS Omega* **2019**, *4*, 9150.
[26] P. Y. Shen, X. M. Li, F. Cao, X. W. Ding, X. Y. Yang, *J. Mat. Chem. C* **2018**, *6*, 9642.
[27] S. Hu, W. Xiang, B. Liu, L. Zhang, G. Zhang, M. Guo, J. Yang, Y. Ren, J. Yu, Z. Yang, *Appl. Phys. Rev.* **2024**, *11*, 021428.
[28] Y. Zhu, Y. Deng, P. Bai, X. Wu, Y. Yao, Q. Liu, J. Qiu, A. Hu, Z. Tang, W. Yu, *Adv. Mat.* **2023**, *35*, 2305382.
[29] I. Bozkaya, Solution-processed/evaporation-based light-emitting diodes of face-down/edge-up oriented colloidal quantum wells, Bilkent University, **2023** https://hdl.handle.net/11693/113820.
[30] W. K. Bae, L. A. Padilha, Y.-S. Park, H. McDaniel, I. Robel, J. M. Pietryga, V. I. Klimov, *ACS Nano* **2013**, *7*, 3411.
[31] J. Luo, L. Han, N. N. Kariuki, L. Y. Wang, D. Mott, C. J. Zhong, T. He, *Chem. Mater.* **2005**, *17*, 5282.
[32] U. Kurtan, H. Erdemi, A. Baykal, H. Güngünes, *Ceram. Int.* **2016**, *42*, 13350.
[33] L. T. Kunneman, J. M. Schins, S. Pedetti, H. Heuclin, F. C. Grozema, A. J. Houtepen, B. Dubertret, L. D. Siebbeles, *Nano Lett.* **2014**, *14*, 7039.
[34] Z. Chen, B. Nadal, B. Mahler, H. Aubin, B. Dubertret, *Adv. Funct. Mat.* **2014**, *24*, 295.
[35] R. Momper, H. Zhang, S. Chen, H. Halim, E. Johannes, S. Yordanov, D. Braga, B. Blulle, D. Doblas, T. Kraus, M. Bonn, H. I. Wang, A. Riedinger, *Nano Lett.* **2020**, *20*, 4102.
[36] K. H. Lee, J. H. Lee, W. S. Song, H. Ko, C. Lee, J. H. Lee, H. Yang, *ACS Nano* **2013**, *7*, 7295.
[37] X. Zhang, H. Lin, H. Huang, C. Reckmeier, Y. Zhang, W. C. Choy, A. L. Rogach, *Nano Lett.* **2016**, *16*, 1415.
[38] F. Shabani, H. Dehghanpour Baruj, I. Yurdakul, S. Delikanli, N. Gheshlaghi, F. Isik, B. Liu, Y. Altintas, B. Canımkurbey, H. V. Demir, *Small* **2022**, *18*, 2106115.
[39] Q. Su, H. Zhang, S. M. Chen, *Npj Flex. Elect.* **2021**, *5*, 8.
[40] C. Zou, Y. Liu, D. S. Ginger, L. Y. Lin, *ACS Nano* **2020**, *14*, 6076.
[41] C. H. Bi, J. C. Hu, Z. W. Yao, Y. Lu, D. Binks, M. L. Sui, J. J. Tian, *Adv. Funct. Mat.* **2020**, *30*, 2005990.
[42] D. Andrzejewski, R. Oliver, Y. Beckmann, A. Grundmann, M. Heuken, H. Kalisch, A. Vescan, T. Kümmell, G. A Bacher, *Opt. Mater.* **2020**, *8*, 2000694.
[43] Y. Wang, Y. Teng, P. Lu, X. Y. Shen, P. Jia, M. Lu, Z. F. Shi, B. Dong, W. W. Yu, Y. Zhang, *Adv. Funct. Mat.* **2020**, *30*, 1910140.
[44] X. Dai, Z. Zhang, Y. Jin, Y. Niu, H. Cao, X. Liang, L. Chen, J. Wang, X. Peng, *Nature* **2014**, *515*, 96.
[45] J. Song, O. Wang, H. Shen, Q. Lin, Z. Li, L. Wang, X. Zhang, L. S. Li, *Adv. Funct. Mat.* **2019**, *29*, 1808377.
[46] S. Scholz, D. Kondakov, B. Lussem, K. Leo, *Chem. Rev.* **2015**, *115*, 8449.
[47] B. Liu, M. Sharma, J. Yu, S. Shendre, C. Hettiarachchi, A. Sharma, A. Yeltik, L. Wang, H. Sun, C. Dang, *Small* **2019**, *15*, 1901983.
[48] F. Qin, M. Lu, S. Sun, P. Lu, N. Feng, Y. Gao, X. Bai, Z. Wu, J. Hu, Y. Zhang, *IEEE Electron Device Lett.* **2023**, *44*, 1056.
[49] L. Liu, H. Yang, Z. Zhang, Y. Wang, J. Piao, Y. Dai, B. Cai, W. Shen, K. Cao, S. Chen, *ACS Appl. Mater.& Interfaces* **2023**, *15*, 21344.
[50] B. Liu, G. Lu, R. Wu, S. Hu, L. Zhang, M. Guo, Z. Yuan, Q. Xue, P. Xiao, D. Luo, *Adv. Opt. Mat.* **2023**, *11*, 2202894.
[51] X. Qian, Y. Shen, L.-J. Zhang, M. Guo, X.-Y. Cai, Y. Lu, H. Liu, Y.-F. Zhang, Y. Tang, L. Chen, *ACS Nano* **2022**, *16*, 17973.
[52] S. Sun, P. Jia, M. Lu, P. Lu, Y. Gao, Y. Zhong, C. Tang, Y. Zhang, Z. Wu, J. Zhu, *Adv. Funct. Mat.* **2022**, *32*, 2204286.
[53] C. Chen, T. Xuan, Y. Yang, F. Huang, T. Zhou, L. Wang, R.-J. Xie, *ACS Appl. Mater. & Interfaces* **2022**, *14*, 16404.
[54] Y. Liu, Z. Yu, S. Chen, J. H. Park, E. D. Jung, S. Lee, K. Kang, S.-J. Ko, J. Lim, M. H. Song, *Nano Energy* **2021**, *80*, 105511.
[55] Y. Liu, L. Zhang, S. Chen, C. Liu, Y. Li, J. Wu, D. Wang, Z. Jiang, Y. Li, Y. Li, *Small* **2021**, *17*, 2101477.
[56] H. Kang, S.-R. Choi, Y.-H. Kim, J. S. Kim, S. Kim, B.-S. An, C.-W. Yang, J.-M. Myoung, T.-W. Lee, J.-G. Kim, *ACS Appl. Mater. Interfaces* **2020**, *12*, 39479.
[57] M. K. Choi, J. Yang, D. C. Kim, Z. Dai, J. Kim, H. Seung, V. S. Kale, S. J. Sung, C. R. Park, N. Lu, *Adv. Mat.* **2018**, *30*, 1703279.
[58] Y. Sun, W. Chen, Y. Wu, Z. He, S. Zhang, S. Chen, *Nanoscale* **2019**, *11*, 1021.
[59] L. Xue, Y. Liu, F. Li, K. Sun, W. Chen, K. Yang, H. Hu, J. Lin, H. Chen, Z. Yang, *Vacuum* **2019**, *163*, 282.

[60] W. Jiang, S. Lee, K. Zhao, K. Lee, H. Han, J. Oh, H. Lee, H. Kim, C. M. Koo, C. Park, *ACS Nano* **2022**, *16*, 9203.
[61] D. C. Kim, H. Yun, J. Kim, H. Seung, W. S. Yu, J. H. Koo, J. Yang, J. H. Kim, T. Hyeon, D.-H. Kim, *Nat. Electronics* **2021**, *4*, 671.
[62] S. Shendre, S. Delikanli, M. Li, D. Dede, Z. Pan, S. T. Ha, Y. H. Fu, P. L. Hernández-Martínez, J. Yu, O. Erdem, *Nanoscale* **2019**, *11*, 301.
[63] R. Scott, J. Heckmann, A. V. Prudnikau, A. Antanovich, A. Mikhailov, N. Owschimikow, M. Artemyev, J. I. Climente, U. Woggon, N. B. Grosse, *Nat. Nanotechnology* **2017**, *12*, 1155.
[64] H. D. Baruj, I. Bozkaya, B. Canimkurbey, A. T. Isik, F. Shabani, S. Delikanli, S. Shendre, O. Erdem, F. Isik, H. V. Demir, *Small* **2023**, *19*, 2206582.
[65] Y. Zeng, W. Yu, Y. Liu, W. Chen, Q. Wang, F. Cao, J. Wei, F. Liu, X. Yang, H. Li, *Adv. Mat.* **2024**, *37*, 2415569.